PointNLM: Point Nonlocal-Means for vegetation segmentation based on middle echo point clouds

Jonathan Li[a,b#], Rongren Wu[a#], Yiping Chen[a]*, Qing Zhu[a], Zhipeng Luo [a]*, Cheng Wang[a]

[a] *Fujian Key Laboratory of Sensing and Computing for Smart Cities, Xiamen University, Xiamen, Fujian 361005, China.*
[b] *Departments of Geography and Environmental Management and Systems Design Engineering, University of Waterloo, Waterloo, ON N2L 3G1, Canada*

Abstract

Middle-echo, which covers one or a few corresponding points, is a specific type of 3D point cloud acquired by a multi-echo laser scanner. In this paper, we propose a novel approach for automatic segmentation of trees that leverages middle-echo information from LiDAR point clouds. First, using a convolution classification method, the proposed type of point clouds reflected by the middle echoes are identified from all point clouds. The middle-echo point clouds are distinguished from the first and last echoes. Hence, the crown positions of the trees are quickly detected from the huge number of point clouds. Second, to accurately extract trees from all point clouds, we propose a 3D deep learning network, PointNLM, to semantically segment tree crowns. PointNLM captures the long-range relationship between the point clouds via a non-local branch and extracts high-level features via max-pooling applied to unordered points. The whole framework is evaluated using the Semantic 3D reduced-test set. The IoU of tree point cloud segmentation reached 0.864. In addition, the semantic segmentation network was tested using the Paris-Lille-3D dataset. The average IoU outperformed several other popular methods. The experimental results indicate that the proposed algorithm provides an excellent solution for vegetation segmentation from LiDAR point clouds.

Keywords*:* Nonlocal Means, Vegetation Segmentation, Multi-waveform LiDAR, Middle-echo Point Clouds, PointNLM Network

#indicates equal contributions.

*Corresponding author at: Fujian Key Laboratory of Sensing and Computing for Smart Cities, School of Information Science and Engineering, Xiamen University, China.

E-mail address: chenyiping@xmu.edu.cn (Y. Chen).

1. Introduction

LiDAR is an active remote sensing technique providing direct measurement of land surfaces via a laser pulse. Full-waveform LiDAR returns multi-echoes, which knock out the whole beam when the launched beams touch the edges of trees or other solid surfaces. The other part of the broken beam continues until it hits the last surface. This phenomenon is characteristic of the penetration of LiDAR. The main advantage of full waveform LiDAR, compared with aerial photography or multi-spectral imaging, is laser beams penetrate the forest canopy. Benefitting from this penetrability, canopy and terrain heights can be acquired simultaneously. Quantitative measures, such as heights, can be measured directly, and the vertical distribution of scatters can be extracted. Since 2004, as shown in Fig.1, so-called Full-WaveForms (FWF) of Airborne Laser Scanning (ALS) systems, which allow recording the entire backscattered waveform of the transmitted laser pulses, have been proposed(Hollaus et al., 2009).

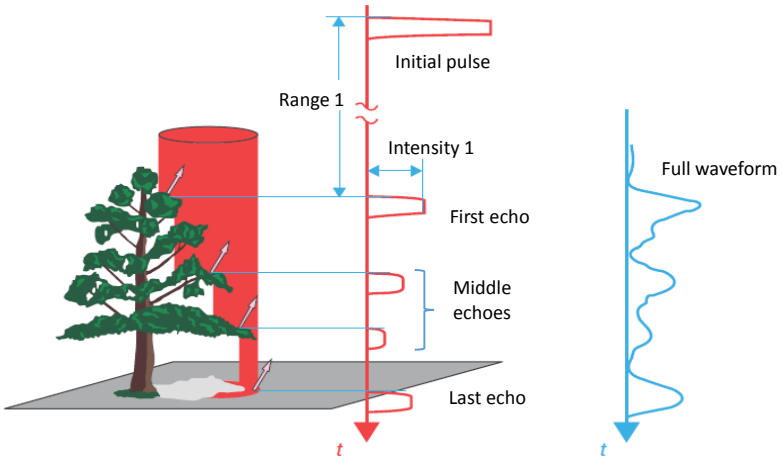

Fig. 1. Illustration of the multi-echo and full-waveform (Vosselman and Maas, 2011)

As the cost of acquiring LiDAR point clouds has decreased, attention has been directed to research on extracting trees from 3D point cloud data. Liu et al. (2017) presented a method to automatically extract, from Mobile Laser Scanning (MLS) point clouds, urban roadside trees, which include ground-removing, clustering, crown seed selecting and growing. Zou et al. (2017) proposed a voxel-based deep learning method to classify tree species collected from complex forest scenes in 3D point clouds. Individual trees are extracted based on the density of the point clouds. Wu et al. (2016) developed an

automated segmentation method to fully utilize LiDAR data and a graph theory-based localized contour for detecting, extracting, and characterizing individual tree crowns.

Huang et al. (2015) proposed a method for automated extraction of street trees in a typical urban environment from 3D point cloud data acquired by a mobile laser scanning system. Statistical component features and horizontal information are calculated for object detection. Nevertheless, it is difficult to deal with the slopes. Guan et al. (2015) addressed the problem of extracting and classifying tree species from mobile LiDAR data; voxel-based upward-growing filtering and Euclidean distance clustering are used in tree extraction. However, all these methods are based on all the point clouds and their basic properties not on the information of the middle echo.

To extract 3-D light poles and trees from Mobile Laser Scanning (MLS) point clouds in a typical urban street scene, Yu et al. (2013) developed a pairwise 3D shape context for partial object matching and retrieval. However, due to the pairwise scheme, the construction of the pairwise 3-D shape context is slower than that of the single-point-based 3-D shape context. Usually, most methods, using LiDAR value-based altitude data to estimate and recognize trees, are not suitable for urban areas because of the different heights of buildings and staggered tree distribution.

Therefore, in this paper, we focus on the segmentation of trees, boscages, and high grass, which are summarized as vegetation. Our algorithm achieves an overall accuracy of 86.4% with the Semantic3D dataset. And it is also applicable to either non-city areas or urban environments, especially complex environments with large-scale mass points.

The contributions of this paper are as follows:

1) We discover the distribution feature of middle echo point clouds and propose a tree crown detection method to effectively and quickly acquire areas of trees and their surroundings from large-scene point clouds by identifying points distributed similarly to middle echo points.

2) Inspired by the Nonlocal Means algorithm in image denoising, we construct a Point Nonlocal Means Network that captures the relationship between two supervoxels that are far removed from each other. Besides, the module of the max-pooling operation is designed for disordered point clouds; thus, the network has a wider receptive field and can capture high-level features of points. Using this network, tree points are accurately segmented from the nearby trees.

The rest of this paper is organized as follows: Related work is discussed in Section 2. The datasets used in this work are presented in Section 3. Methods are

given in Section 4. Tree detection and segmentation are discussed in Section 5. The conclusion is provided in Section 6.

2. Related Work

2.1. Based on geometric rules

Rule-based methods generally detect and extract trees using special geometric rules such as tree shape, cylindrical trunk, point cloud distribution, etc. They can be divided into three classes: the clustering based methods, region growing based methods, and density thresholds based methods. Babahajiani et al. (2017) proposed a algorithm that takes GPS registered LiDAR point clouds and street view images as inputs and creates, using a hybrid of rule-based parsing, semantic labels for large 3D object points. The complex structures of cars, trees, pedestrians, etc. are divided into small supervoxels. Then, distance and main direction, used as super-voxels similar to the regional combination, are finally classified by supervised learning. There is no mention of applicability to large-scale visualization of point cloud scenarios. Xu et al. (2018a) proposed a method for adaptively filtering ground points and constructing an elevation histogram based on elevation information. Then, a point cloud between 120 and 160 cm from the ground is intercepted and projected onto the XY plane. A candidate tree is detected by circle detection. Finally, a dynamic programming algorithm extracts the complete tree. It is a traditional method and not competitive in speed. Yang et al. (2015) proposed a method that generates multi-scale supervoxels from 3D point clouds using the point attributes and spatial distances between points and then segments the supervoxels, rather than individual points, by combining graph-based segmentation with multiple cues of the supervoxels. Their method defines a set of rules for merging segments into meaningful units according to types of urban objects and forms the semantic knowledge of urban objects to classify objects. Xu et al. (2018b) proposed a bottom-up hierarchical segmentation algorithm to merge non-photosynthetic point cloud clusters. The clusters are combined according to the difference between two cloud clusters, where the distance matrix is determined by the Euclidean distance and main direction terms. Weinmann et al. (2017) proposed a method that first uses geometric features for a binary point-wise semantic classification with the objective of assigning semantic class labels to irregularly distributed 3D points and, second, passes the labels through semantic segmentation with the objective of separating individual trees within the tree points.

However, all of the above methods are difficult to segment the trees from areas of dense mixed objects in large-scale scenes. Because the local geometric

features of each point need heavy computing costs. Our method with the help of middle-echo information can quickly get all the existing penetrating foliage for a wide range of scenarios.

2.2. Based on semantic segmentation

2.2.1. Projection to multiple view images

The multi-view depth learning method for 3D point clouds, which creates twelve rendered views representing 3D data by placing twelve virtual cameras around the grid every thirty degrees, is the result of groundbreaking research by Su et al. (2015). These images are then used as inputs to a Convolutional Neural Network (CNN) to learn the features of each view, and the view features are merged and passed to another CNN to identify the model. To obtain 2D representation of a 3D point cloud and avoid the view selection problem, Luo et al. (2019) designed three feature descriptors acquired from the following images: horizontal single rotation, vertical volume accumulation, and vertical angle accumulation. The high-level features, extracted by the two-stage fusion network, are used for 3D model road identification. Boulch et al. (2017) applied a 2D convolution to a 2D snapshot of a 3D point cloud and then projected the label back into 3D space.

Their segmentation results of deep neural network are usually required the 2D information, which adds multidimensional registration process. The approach we propose belongs to the single view of point clouds have two key points: we are the first to take advantage of the concept of multiple echoes created by the gaps between the leaves to segment the trees; we synchronize and cover the all range to allow sharing the middle-echo features thus increasing generalizability of our PointNLM.

2.2.2. General voxel and 3 D-CNN

Maturana and Scherer (2015) used 3D volume occupied grids to represent 3D point clouds and supervised 3D CNN to solve 3D point cloud model recognition. These 3D occupied grids include the following grids; binary occupied, density occupied, and hit. The effect of this simple 3D footprint depends highly on the resolution of the grid. The higher the resolution, the finer the effect when splitting the task. As voxel resolution increases, memory and computational costs also increase. Spatial division methods, for example, the octree-based method (Riegler et al., 2017) and the KD tree method (Klokov and Lempitsky, 2017) were proposed to solve this problem.

2.2.3. Point-wise segmentation

C. R. Qi et al. (2017a) proposed PointNet, a neural network that first directly consumes point clouds and can be applied to raw point cloud data. However, before performing max-pooling, PointNet processes each point identically and independently. Therefore, PointNet is not suitable for multi-classification problems having multiple instances. To overcome this drawback, C. R. Qi et al. (2017b) used a hierarchical approach to capture local structures, as well as generalize the variable densities, thereby solving the problem of uneven sampling and considering also the distance metric between points in space. The hierarchical structure is used to learn features by using local area information; the network structure is more effective and robust. C. Wang et al. (2018), to leverage the power of spectral GCNNs in the PointNet++ framework, proposed graph convolution to deal with unordered point clouds. To solve the problems of a huge volume of point cloud data and quantification of artifacts, Te et al. (2018) proposed a method in which a Regularized Graph Convolutional Neural Network (RGCNN) directly consumes point clouds, significantly reducing computational complexity. To introduce CNNs into the classification and segmentation of point cloud data, Hua et al. (2018) presented a CNN for semantic segmentation and object recognition in 3 D point clouds.

2.2.4. Patch-wise segmentation

Point-wise indoor point cloud segmentation has achieved quite good results. However, because of the huge amount of data in outdoor scene point clouds, these network models are rarely used for point cloud processing of such a level of data. One way to deal with a large number of point clouds is to over segment the point cloud data into a number of patches before point cloud semantic segmentation. Then, based on these small blocks, semantic segmentation is performed. Landrieu and Simonovsky (2018) split the outdoor large scene point cloud into many superpoints. The points in each superpoint are geometrically consistent. Then, the superpoints are input into a network, which uses PointNet to extract the features of the superpoints, uses the GRU network to extract the relationship between these super points, and finally, to complete segmentation, classifies each superpoint. (Luo et al., 2018) segmented the MLS point cloud of a road scene into supervoxels, and then (human-machine) interactively labeled a small part of the supervoxels for training the active learning labeling model conditional random field.

However, the above methods require high memory and computational cost as the voexl resolution increases. What's worse, these methods rely on subdivision of a bounding volume rather than local geometric structure, which is very

important for extracting deep 3D shape features. Different from the way of representing 3D data, in our work, we combine the Non-local Means idea and the point based network to design our method, the PointNLM, to capture the relationship between two supervoxels that are far removed from each other.

3. Methods

In this section, we present a 3-step tree segmentation method. First, the tree regions are obtained by finding points with a distribution similar to that for middle echo points (Section 4.1). Second, the extracted tree regions are represented by supervoxels (Section 4.2). Third, the supervoxels belonging to trees are segmented by our PointNLM Network (Section 4.3). Besides, the labels are interpolated to assign the labels back to points and maintain the tree points.

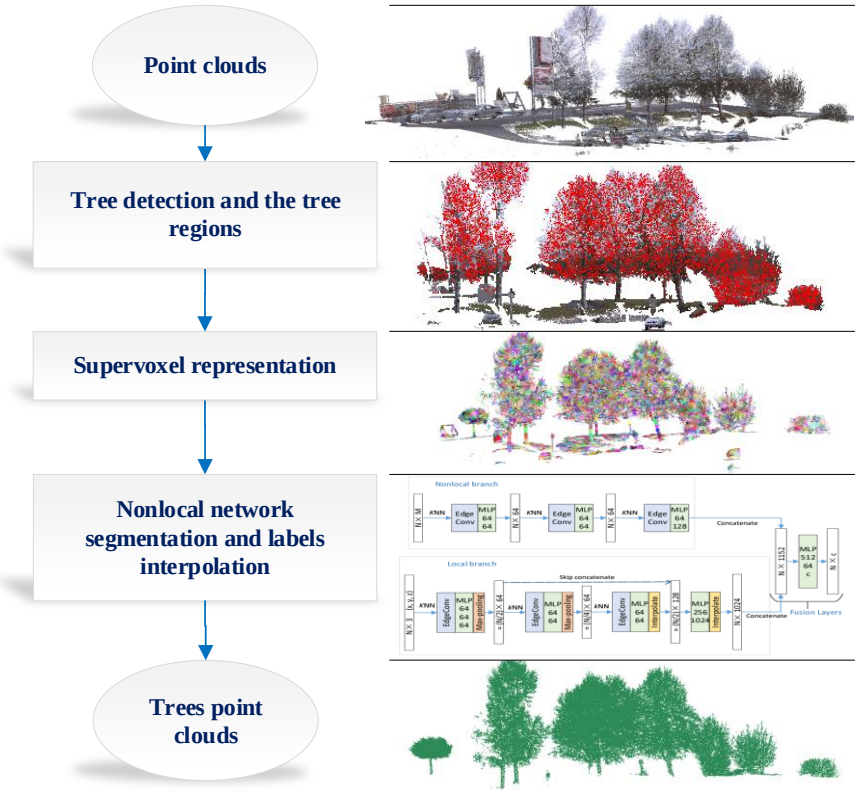

Fig. 2. Flowchart of the proposed tree segmentation method.

3.1. Middle echo points for trees detection

The Terrestrial Laser Scanning (TLS) system we used has the characteristic of penetration and capability to record multi-echoes on the canopy and transparent objects. Besides, the middle echo points, which are two orders of magnitude smaller in number than the entire number of echo points, also retain relatively complete canopy information. Hence, we can detect trees by finding points with a distribution similar to that of middle echo points. Different from tree crown points, points reflected from man-made objects are mostly of linear, planar, or curved surface distribution.

Canopy points are detected by the irregular distribution characteristic. The down-sampled point cloud of a point cloud without middle echo points can be used as detector points. The neighboring points of each detector point are extracted to construct local information. For rapid data indexing, a KD-tree structure is constructed among the down-sampled point cloud. Then, we traverse each detector point in turn; when traversing every detector point $\mathrm{P}_i = (\mathrm{x}_i, \mathrm{y}_i, \mathrm{z}_i)^T$, searching its N_{sam} = 24 nearest detector points and N_{row} = 104 nearest points to construct the local points.

Dimensional feature computing, via Principal Component Analysis (PCA), is used to describe the local geometrical characteristics of point clouds (Gross et al., 2007; Demantké et al., 2011; Yang and Dong, 2013), even though it has only a few values, such as eigenvalues, to do so. Inspired by PointNet (C. R. Qi et al., 2017a), which uses points as the direct input of the neural network, we use a CNN to extract a feature vector with dimensions of K = 1,024 for local points. The max-pooling layer is used to acquire a feature vector among the features of the local points to represent the local information. Then, a few fully connected layers are used to determine whether the local points are irregularly distributed and whether the corresponding detector point can be classified as a canopy point.

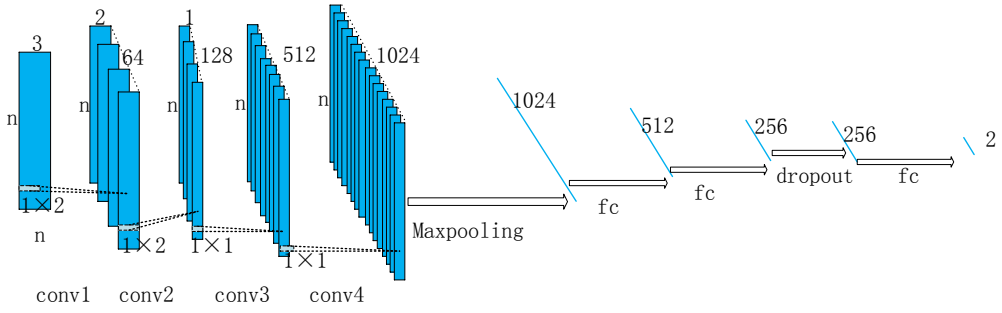

Fig. 3 Architecture of tree detection neural network.

Fig. 3 shows the detailed structure of the tree detection neural network. The network directly takes normalized n points as input, where every point is a

three-dimensional vector with coordinates, (x, y, z). The four convolution layers have the following convolution kernels: $(1, 2)$, $(1, 2)$, $(1, 1)$, $(1, 1)$. After one max-pooling layer, one dropout layer, and three fully connected layers, the network output becomes a two-dimensional vector. If the first element of this vector is the larger one, the input points are irregularly distributed and belong to canopy points. Otherwise, the input points are points belonging to other objects. After going through the network, almost all the canopy points, and a small number of points belonging to other objects, remain. Then, based on distance, we filter out the small number of points belonging to other objects. We finish tree detection by finding points similar to middle echo points.

3.2. Supervoxel and feature

As mentioned before, it takes considerable time and computational resources to point-wise segment an outdoor scene point cloud. Therefore, before the clouds are fed into neural networks, representation and organization of irregular point clouds is quite significant. Unlike the geometric partition with a global energy function proposed by Landrieu and Simonovsky (2018), we chose the Voxel Cloud Connectivity Segmentation (VCCS) algorithm to over-segment point clouds into smaller supervoxels. This algorithm avoids violating object boundaries; therefore, it does not decrease the accuracy of a classifier because points belonging to more than one class are divided into the same patches. In this paper, two parameters, voxel resolution and seed resolution in the VCCS algorithm, are set at 0.07m and 0.14m, respectively.

Because the points within a supervoxel have consistent geometry, a supervoxel can be represented as a feature vector without much loss of information. Some of the features for each supervoxel are as follows:

- The centroid of a supervoxel: $o_i = (x_i, y_i, z_i)$.
- The ratio of middle echo points to points within a supervoxel, which is useful information for tree location.
- The linearity, planarity, and scatter of point distribution in a supervoxel $(\frac{\sqrt{\lambda_1}-\sqrt{\lambda_2}}{\sqrt{\lambda_1}}, \frac{\sqrt{\lambda_2}-\sqrt{\lambda_3}}{\sqrt{\lambda_2}}, \frac{\sqrt{\lambda_3}}{\sqrt{\lambda_1}})$ and some other 3D geometric features (Weinmann et al., 2015).
- The eigenvectors correspond to three eigenvalues.

3.3. Nonlocal Means Network

Given a set of supervoxels represented as $X = \{x_i | i = 1,2,\ldots,n\}$ with $x_i = \{o_i, f_i\}$, where o_i and f_i are the centroid and geometric features of a supervoxel, respectively, the task in this step is to assign each supervoxel a label

selected from the candidate label set $L = \{\ell_1, \ell_2, \ldots, \ell_k\}$. Of course, for the tree extraction problem, k = 2. The architecture of a NonLocal Means (NL-Means) network consists of three main components: non-local branch, local branch, and fusion layers. We use EdgeConv proposed by Y. Wang et al. (2018) as the basic element.

The non-local branch uses the M features (without centroids) of every supervoxel as input; whereas, the input of the local branch is the centroids (x, y, z) of these N supervoxels. The fusion layers are used to concatenate those local features and non-local features and provide a score for every supervoxel. Additionally, kNN means the operation to construct the k nearest neighbor graph. MLP is the multi-layer perceptron, whose layer sizes are given in brackets.

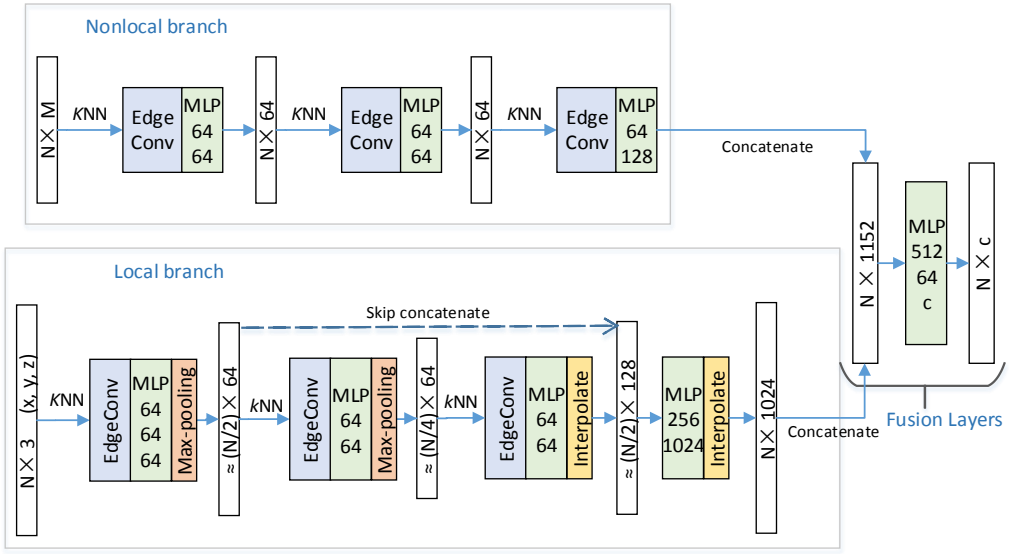

Fig. 4. Architecture of Nonlocal Means Network.

3.3.1. EdgeConv

EdgeConv is a simple operation, which generates edge features that describe the relationship between a point and its k nearest neighbors. Then, Multi-Layer Perceptron (MLP) and max aggregation are used in EdgeConv to capture local geometric structures for that point. EdgeConv outputs a d_1 dimensional point cloud with the same number of points of input data. For more details regarding EdgeConv, see the following: Y. Wang et al.(2018).

Actually, most of the k nearest neighborhood points have consistent 3D geometry and appearance, and, after applying EdgeConv, they have the same d

dimensional features. When applied to every point, EdgeConv performs unnecessary computations and cannot process a large-scene point cloud. Another problem is that the perception field is constrained by the *k* nearest neighborhood points. Only quite deep networks, built by EdgeConv, have a large perception field. Therefore, so the network can process the large-scale point cloud and not repeatedly capture the same feature for neighborhood points, EdgeConv is applied to the supervoxels. Also, we design a network that can capture the remote relationship in the scene.

3.3.2. Non-local branch architecture

The architecture of the non-local branch is inspired by the denoising algorithm, Nonlocal Means (NL-Means), which replaces the noise pixel value with a weighted sum of all pixel values in the image, as follows:

$$\tilde{u}(x) = \sum_{y \in I} w(x, y) v(y) \tag{1}$$

where weight $w(x, y)$ depends on the similarity between the neighborhood structure of two pixels: x, y.

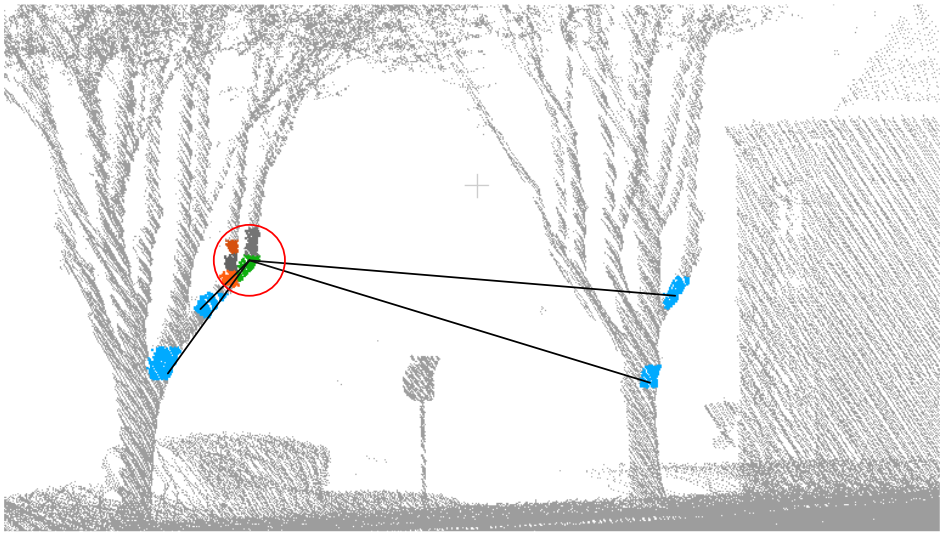

Fig. 5. Local and non-local graph.

The non-local branch of our network is designed to implement, through a neural network, an operation similar to the NL-means algorithm. The features of

all supervoxels, but without the supervoxel positions, are the input for this branch. These features are $= \{f_i | i = 1,2, \dots, n\}$, which were introduced in Section 4.2. Updating these features by directly applying Eq. (1) to the features requires a considerable amount of time. Therefore, in this function, only the features of the k nearest supervoxels are considered. The k nearest neighbor graph, $= \{F, E\}$, is constructed for the features, F, of all supervoxels. For any vertex, f_i , in graph, G, there are edges, $\{e_{ij} | j = 1, \dots, k\}$,between f_i and its k nearest neighborhood vertices, $\{f_{i_j} | j = 1, \dots, k\}$. Because the input of the non-local branch does not include the position, o_i , of the supervoxel, without a spatial constraint, such as the green and blue supervoxels in Fig. 5, the distance between f_i and f_{i_j} can be quite long. For this reason, in our network, we call it a non-local branch. Providing long-range information for the network are edges between the green supervoxel and the far-removed blue ones. However, for the graph of the local branch, only the supervoxels in the red circle are directly connected to the green ones.

EdgeConv, followed by Multi-Layers of Perceptron (MLP), is used to update the vertices of graph G according to the relationship between those vertices and the k most similar vertices. For a vertex, f_i, the updated features, f_i' , are given by the following formula:

$$f_i' = h(f_{i_1}, \dots, f_{i_k}) \tag{2}$$

where $\{f_{i_j} | j = 1, \dots, k\}$ are those vertices having edges to vertex, f_i, and $h()$ is a function implemented by MLP. Particularly, if there is only a fully connected layer, Eq. (2) will be in a simple form, as follows:

$$f_i' = \sum_{j=1}^{k} \theta_{i_j} f_{i_j} \tag{3}$$

where $\{\theta_{i_j} | j = 1, \dots, k\}$ are learnable parameters that play the same role as weight, $w(x,y)$, in Eq. (1). These operations are cascaded three times in the non-local branch, and the graph is reconstructed every time. The new features with the same number of supervoxels are the output of this non-local branch. These new features better describe the shape and geometry of supervoxels for a more exact classification.

3.3.3. Local branch and fusion layers

The base unit of a local branch is the same as that of a non-local branch. However, the input and output of the local branch are totally different. The input is only the centroids, $O = \{o_i | i = 1, \dots, n\}$, of the supervoxels; $o_i = (x_i, y_i, z_i)$ are the 3D coordinates. To construct the k nearest neighbor graph, these points are regarded as vertices. Another difference for the non-local branch is there are max-pooling layers and skipped connections in the local branch. These two components are described in detail in the next subsection. The output of the local branch contains low-level and high-level features. Low-level features are the output of the first few convolution layers. High-level information is the output of the max-pooling layer following the several convolution layers.

The outputs from the local and non-local branches are concatenated as a features vector for every supervoxel. Therefore, low-level, high-level, and long-range information are fused. Finally, multilayer perceptron is used to classify every supervoxel.

3.3.4. Max-pooling and interpolate layers

Y. Wang et al., (2018) proposed a network, which having an output of N points for every layer, uses single max-pooling to obtain global features. There are two shortcomings in this kind of design. One is the network requires more computational resources, thereby limiting the number of points that can be processed. Another is the features of a point can spread only among the nearest neighboring points, which constrains the perception field, unless the network is quite deep.

To deal with these issues, we add pooling layers to the network. The problem is how to pool among point clouds. Actually, C. R. Qi et al. (2017b) proposed a set abstraction model that is similar to pooling. Their model groups some points in 3D coordinates and outputs a feature vector captured by PointNet. We propose another way to perform max-pooling among point clouds.

Our way is to re-order the points based on feature space, then apply max-pooling among the point clouds the same as we do to images. After re-ordering, the points, that are closer in feature space, are placed in adjacent locations. Hence, max-pooling can be performed on adjacent points in the permutation. The size of the pooling kernel is set arbitrarily. The permutation of the points is determined by kernel size, s_k, and features distribution. First, the k_n nearest points in feature space are found for every point, where k_n is not smaller than s_k. Second, we randomly select one point from the points that were not reordered, as well as the other $(s_k - 1)$ points in the k_n nearest points. These s_k points are placed in adjacent locations. If the other not reordered $(s_k - 1)$ points are

insufficient, we add a point with "zero" as features, instead. In max-pooling, "zero" features do not affect the max-pooling result. So the new features can be interpolated back to the original place after max-pooling and multi-layer perceptron, when reordering the points, we record the original point indices.

Suppose, as shown in Fig. 6, there are nine points, whose features are $\{f_i | i = 1,2,\cdots,9\}$, and the distribution of these features is that shown in the picture. Also, the sizes of pooling kernels s_k and k_n are both set at 3. Then, based on their distribution, we reorder these points. First, points "2" may be selected for reordering, and the three nearest points are "2," "1," and "5." Second, these three points are placed so they are adjacent and marked as having been reordered. These two steps are then repeated among those points that have not yet been reordered. When we select point "6," its two nearest points are "3" and "5." However, point "5" has been reordered; therefore, a zero feature takes its place so max-pooling can be applied correctly between points "6" and "3." After reordering, we apply max-pooling with stride as "3" among these points and obtain four new points.

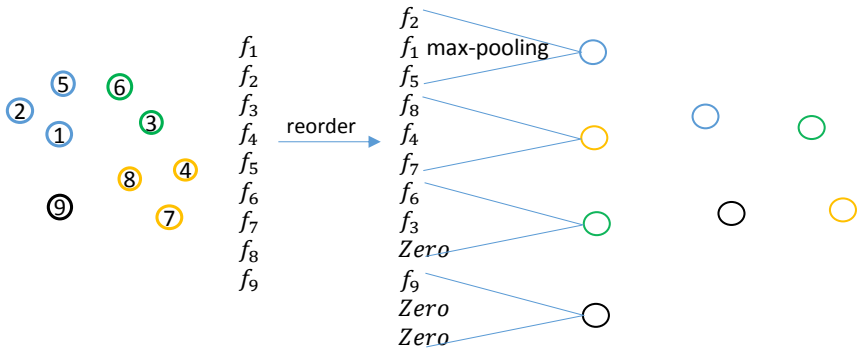

Fig. 6 Illustration of max-pooling operation.

4. Experiments and analysis

Our proposed tree segmentation method can detect tree crown and tree segment points efficiently from complex large-scale scene point clouds. The first proposed middle echo information, based on the tree crown detection method, was applied among large-scene point clouds to quickly acquire tree locations. The PointNLM network was proposed to finely segmenttrees from the region nearby the detected tree locations. To evaluate the effectiveness of our method, we divide our experiments into three parts. First, we evaluate the proposed method using the Semantic 3D dataset, consisting of urban and rural large-scene

point clouds. Second, we evaluate the PointNLM network using the Paris-Lille-3D dataset, which is a benchmark for 3D point cloud segmentation. Third, we test our tree segmentation framework on large-scale point clouds.

4.1. Data with middle echo points for learning local canopy information

Data was acquired by a RIEGL VZ-1000 system in the city of Xiamen. This sensor is a small-footprint Terrestrial Laser Scanning (TLS) sensor, which provides a measurement range of 1.4 km with 5 mm repeatability, and a measurement rate up to 122,000 measurements/sec (about 3,855 points/m2 for the ground). The LiDAR system consisted of echo digitization and online waveform processing. According to the characteristics of laser scanner pulse penetration and capability of multi-echo recording, laser beams easily pass through a canopy of deciduous trees. Penetration index, a function of canopy density, decreases with increased canopy density. In a scene of point cloud data, the middle echo is defined as the penetration layer, or zone of penetration. Because these middle echo points belong mostly to the canopy, we learn local information about the canopy from the middle echo points and detect vegetation in a large-scale scene.

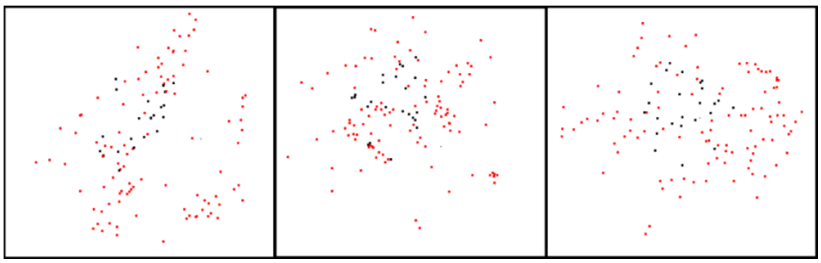

Fig. 7. Different views of a middle point's local distribution.

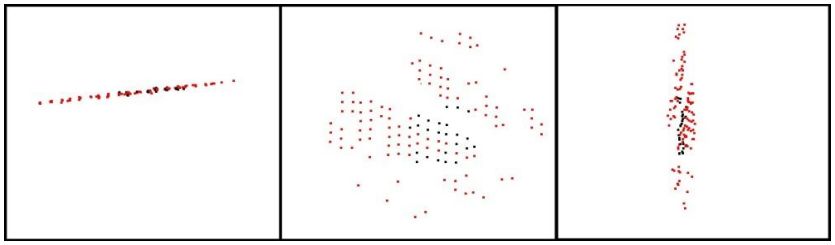

Fig. 8. Different views of one other object point's local distribution.

We created a local dataset from the multi-echo point clouds acquired by the RIEGL VZ1000 TLS system. The local dataset consists of nearly thirty thousand samples, labeled "0" (middle echo point distribution) or "1" (non-middle echo

point distribution). This local dataset was constructed from several scenes in Xiamen. Each sample consists of 128 points. Fig. 7 and Fig. 8 show the different views of these two different distributions of local point data.

4.2. Semantic3D dataset

The entire tree segmentation method we proposed is evaluated using the Semantic3D dataset (Hackel et al., 2017), which is a large-scale point cloud classification benchmark. This dataset consists of high-precision dense point clouds collected by a static ground laser scanning system in Central Europe. The Semantic 3D dataset provides point cloud data, totaling more than four billion points, for a variety of large-scale outdoor scenes in urban and rural areas. Each point has spatial coordinates (x, y, z), intensity information, RGB color information, and a manually assigned corresponding label. All point clouds, covering a wide range of urban outdoor scenes, are divided into eight categories: man-made terrain, natural terrain, high vegetation, low vegetation, buildings, remaining hard scape, scanned artifacts, and cars. In this experiment, we focus on the high vegetation in these eight types of objects and also detect low vegetation point clouds and distinguish them from high vegetation. There are fifteen different scenes, including urban, suburban, and rural in the training dataset, and four scenes in the small testing set.

4.2.1. Tree detection

As described in Section 4.1, the tree positions are first detected by finding points similar to middle echo points. Hence, the tree detection neural network (5) is trained by the local datasets we created. Then, the trained model is used to locate tree positions in the Semantic3D dataset, including both the training and testing sets. The point clouds in Semantic 3Dare down-sampled and used as detector points. These detector points, according to their local distribution, are classified by the trained model. After locating trees, the approximate areas around the trees are extracted for further processing.

Fig. 9 shows the canopy detection results for the proposed tree detection method in two test scenes. The first picture is a rural scene point cloud with relatively more trees; the second picture was collected from an urban scene. This figure shows the effect of superimposing the detector points discriminated as the crown on the original colored point cloud; the red point is the point cloud detected as the crown. The enlarged areas in the figures show some nearby areas extracted according to the detected canopies. As shown in Fig. 9, the proposed canopy detection method effectively detects the positions of the canopies from a large-scene point cloud, whether it is an urban or a rural scene. Only a few objects, such as eaves or windows are detected as canopy point clouds. These

objects and those in the vicinity of the canopy are removed in the next step of the tree segmentation.

4.2.2. Tree segmentation

Until now, we have rough areas that could be trees. These areas often include ground, humans, and vehicles under the trees, as well as some other objects mistakenly detected as trees. More than a thousand suspected trees are detected in fifteen training scenarios. The points in suspicious areas on these training sets are labeled as trees, bushes, or other and then used to train our proposed PointNLM network.

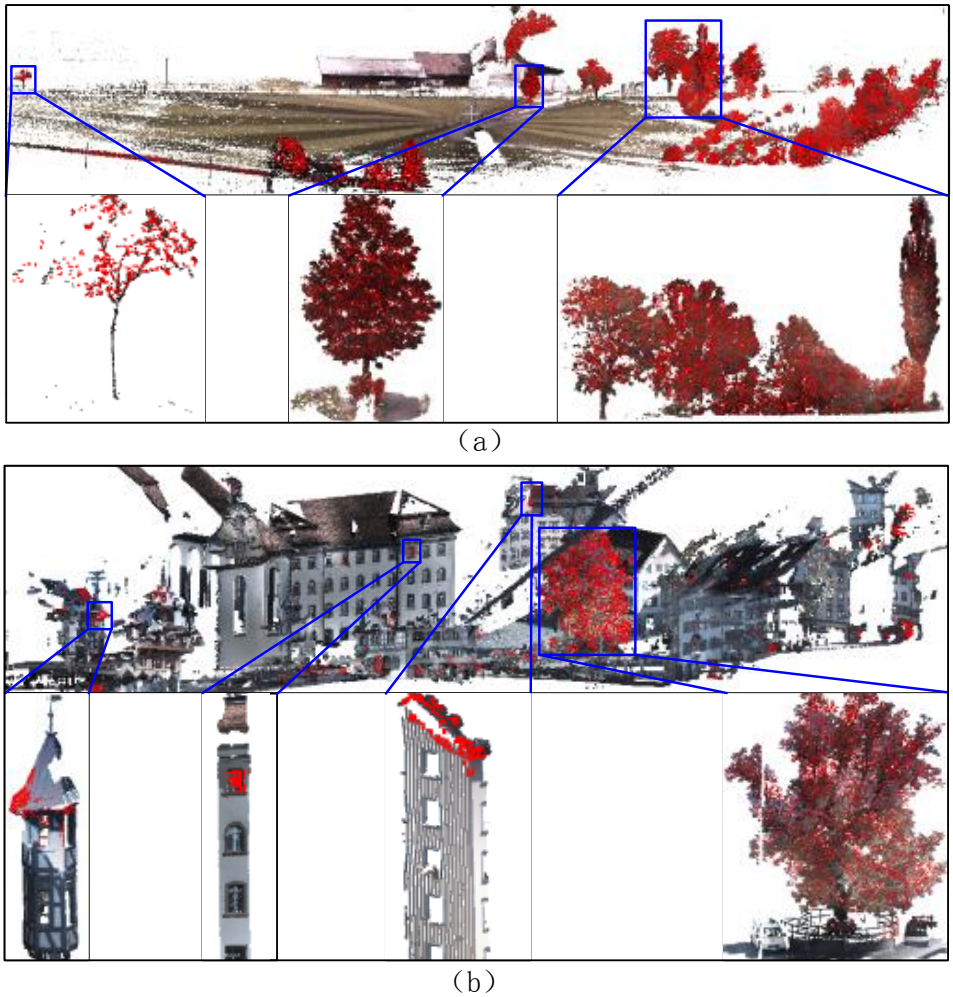

Fig. 9 Trees detection results of two scenes in the test dataset (Red: detector points classified as tree points, showing some nearby areas extracted according to the detected canopies).

Before being used in a training network, these suspicious areas must be normalized, which is an operation that greatly influences the model training. However, when normalizing these suspicious areas, two parameters must be properly set. One is the translation parameter used to move the region to the origin. If we directly use the lowest point of an area as the new origin, the classification result of the suspended tree crown or roof caused by obscuring other objects will be affected. If the lowest point of the entire scene is used as the amount of translation on the Z axis, the segmentation of the suspicious area on the higher slope will be affected. Therefore, the translation value on the Z-axis for one suspicious area is set as the height of the lowest point among its three nearest suspicious areas. The other is the scaled value used to ensure that the point coordinates lie between zero and one. This value is set as the highest of all suspicious areas in one scene. However, some isolated special points that are more than 100 meters high in some scenes must be removed first.

Therefore, the normalized coordinates of the point, $= (x_i, y_i, z_i)$, in the vicinity of a canopy are obtained as follows:

$$p_i' = (\frac{(x_i - x_{min})}{s}, \frac{(y_i - y_{min})}{s}, \frac{(z_i - z_{min3})}{s}) \quad (4)$$

where z_{min3} is the Z value of the lowest point of the three nearest regions of the suspicious area; $x_m in$ and $y_m in$ are the minimum values of the suspicious area on the X-axis and the Y-axis, respectively; s is the maximum height difference in the scene.

Then, we evaluated the tree segmentation results from the suspicious areas in the testing set. The points in the scene, that are not in suspicious areas, are directly assigned their labels with the others. To correctly upload the tree segmentation results from the four test scenarios to the Semantic 3D official website and compare them with the official unpublished real tags, we tagged the following in the Semantic 3D dataset: "3 (high vegetation)," "4 (low vegetation)," and "5 (buildings)" for trees, bushes, etc. Fig. 10 shows the results of the tree segmentation in two test scenes. In the picture, green points belong to the tree; blue is the point cloud of the bushes; gray is other objects. In addition, the enlarged areas in the figures show the semantic segmentation results of those suspicious areas. As shown in Fig. 10, the tree segmentation algorithm achieved quite good segmentation results, both in the first rural scene and in the second urban scene.

Finally, from the Semantic 3D website, we obtained the segmentation results for the four test scenes i.e. the classification confusion matrix. In Table 1, L1' to

L8' represent the predicted labels for artificial ground, natural ground, high vegetation (tree), low vegetation, buildings, hardscapes, scanned artifacts, and trucks. Values for the columnar Li through Lj (L1 through L8) entries are the number of points having ground truth label i, but are predicted by the model as label j.

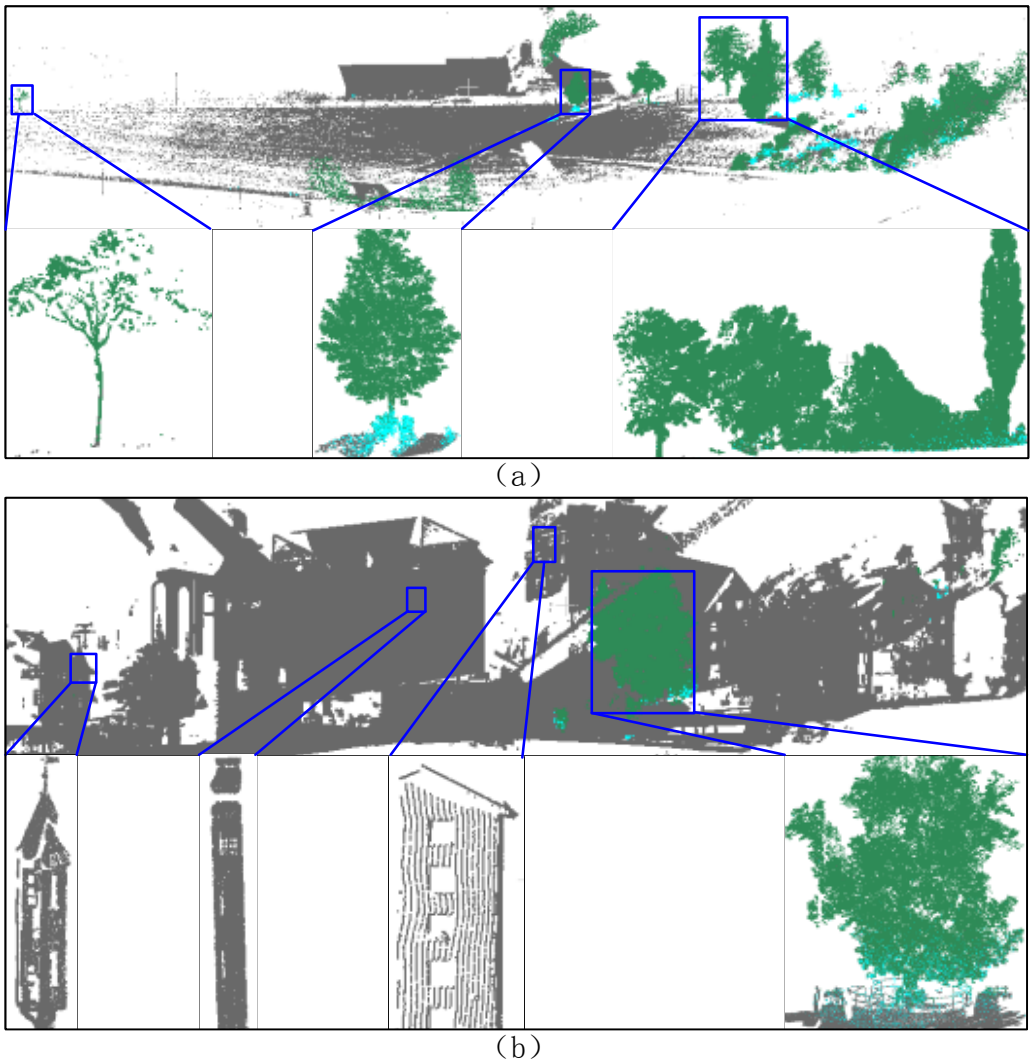

Fig. 10 Trees segmentation results of two scenes in the test dataset (green: trees points; blue: bushes points; gray: other objects).

Intersection over Union (IoU) was used to evaluate the segmentation results. Suppose that the labels of various point clouds are represented by integers {1, 2..., L}, where L is the number of categories; the matrix M with size L×L

represents the confusion matrix of the classification result. Then the IoU for category i is calculated as follows:

$$IoU_i = \frac{M_{ij}}{M_{ij} + \sum_{j \neq i} M_{ij} + \sum_{k \neq i} M_{ki}} \tag{5}$$

Table 1：Confusion matrix of Semantic 3D test set

Prediction / Ground truth	L1’	L2’	L3’	L4’	L5’	L6’	L7’	L8’
L1	0	0	1618	164125	14151766	0	0	0
L2	0	0	2861	9140	10682745	0	0	0
L3	0	0	4479080	58825	137966	0	0	0
L4	0	0	376281	863399	1782214	0	0	0
L5	0	0	81069	19986	30810151	0	0	0
L6	0	0	44340	118849	2221356	0	0	0
L7	0	0	3017	8701	222121	0	0	0
L8	0	0	79	41496	810367	0	0	0

Table 2: IoU of tree segmentation in Semantic 3D dataset

Method	SPGraph	Ours	SEGcloud	RF MSSF	SnapNet	DeePr3ss
IoU(tree)	0.879	0.864	0.860	0.818	0.797	0.742

Table 2 shows results generated by our methods and other state-of-the-art methods. As seen from the table, our algorithm achieves better results than the SEGcloud, which uses a neural network based on voxels. Besides, our IoU is also higher than SnapNet, which applies a neural network to images transformed from point clouds.

Our score is a little lower than that for SPGraph, probably because some quite sparse points, that cannot be represented well in supervoxels, are misclassified. Another reason is that over 0.37 million bush points are misclassified into high vegetation point clouds, which reduces IoU by 10 %. Solving this problem will be one of our future work.

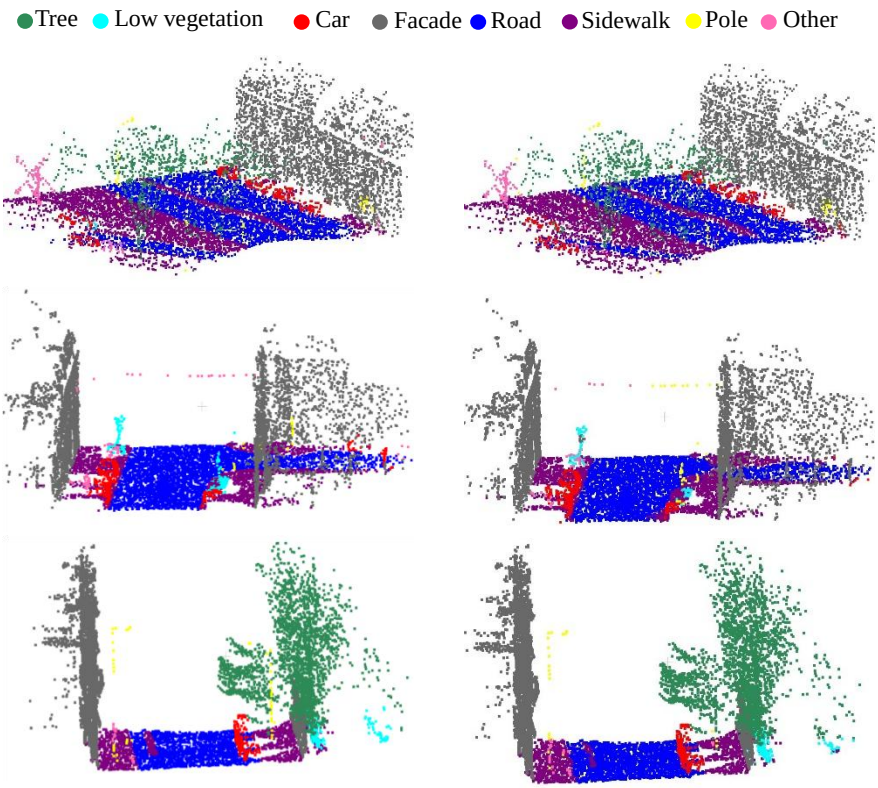

(a) Ground truth (b) Prediction

Fig. 11. Example visualization results on Paris-Lille-3D dataset (dots: centroids of supervoxels showing 4 point size in CloudCompare).

4.3. Paris-Lille-3D dataset

We evaluated the Point Nonlocal Means Network on the Paris-Lille-3D dataset (Roynard et al., 2017), which is an urban point cloud dataset for semantic segmentation acquired by mobile laser scanning. This dataset covers about 2 km (three sections) along the road and has been labeled with fifty different classes. To reduce the size of the scene，the network quickly detects the tree feature-based point clouds from large-scale scenes. The point clouds in the three sections are separated into 69 sections, which are about 30 m per section along the road. Fifty-seven sections are used to train the network; twelve are used for testing. Besides, some of the fifty classes rarely appear in the dataset and have very few points. Therefore, the same as for most datasets, we merge these classes into only the following eight classes: facade, tree, pole, low vegetarian, road, sidewalk, car, and others.

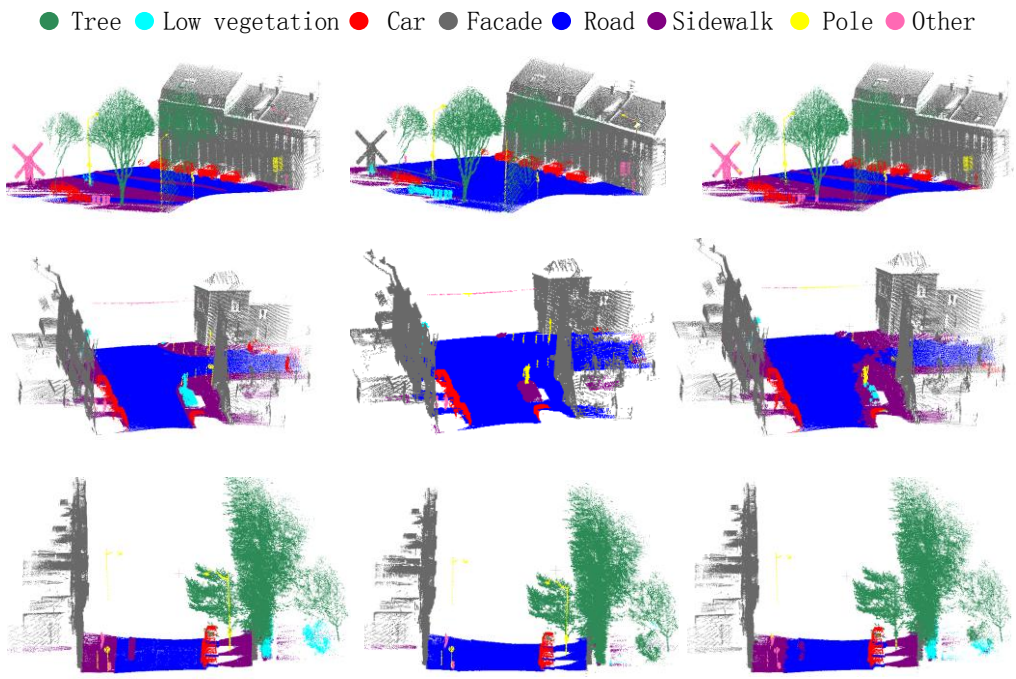

(a) Ground truth (b)SPGraph (c)PointNLM (ours)

Fig. 12 Example results after label interpolation on Paris-Lille-3D dataset.

After the supervoxel segmentation by the VCCS algorithm, the number of supervoxels in a section point cloud varies with different scenes. To batch process these point cloud sections, during training and testing, we sample a fixed number of supervoxels from the scenes in each section. During sampling, N_{sv} supervoxels are randomly chosen without repetition. If the number of supervoxels is insufficient (N_{sv}) we repeat some supervoxels until there is enough (N_{sv}). Besides, the centroids of the supervoxels, $o_i = (x_i, y_i, z_i)$, in every scene are normalized as follows:

$$o_i' = \left(\frac{2(x_i - x_{min})}{x_{max} - x_{min}} - 1, \frac{2(y_i - y_{min})}{y_{max} - y_{min}} - 1, \frac{2(z_i - z_{min})}{z_{max} - z_{min}} - 1\right) \quad (6)$$

where x_{min}, y_{min}, and z_{min} are the minimum coordinate values of the scene on the X, Y, and Z axes, respectively; x_{max}, y_{max}, and z_{max} are the maximum coordinate values of the scene on the X, Y, and Z axes, respectively.

The proposed PointNLM Network is illustrated in Fig. 6. There are three EdgeConv layers, two Max-pooling layers, and one skip connection. The parameter for the *k* nearest neighbor is set as 20. The max-pooling kernel is set

as (2, 1). The number of points, after max-pooling, is about half the number as before max-pooling.

The prediction results of some of the superevoxel scenes are shown in Fig. 11. As seen, most of the large objects are predicted correctly; whereas, for objects with sparse points, error in prediction occurs. Then, we interpolate the labels of the supervoxels to all the original points. Some prediction results for all points (Fig. 12) illustrate that our network performs well among most objects, except for road edges and quite small objects.

We used overall accuracy and mean IoU to evaluate our method quantitatively and compared it with two other methods. As shown in Table 3, on the twelve test scenes, our method performs far better than the SPGraph. From Table 4, it is seen that the major improvement in scores is for the more accurate classification of road and sidewalk, because SPGraph cannot separate these two classes in the geometric partition process. In addition, our network performs better than DGCNN, indicating that non-local branches and maximum pool operations are useful. The greater the point cloud density, the more pronounced the impact of the largest pool.

Table 3: Overall accuracy and mean intersection over union metric of Paris-Lille-3D dataset

Method	Overall Accuracy (%)	mean IoU (%)
SPGraph	85.49	65.28
DGCNN	95.41	78.62
PointNLM (ours)	**96.25**	**80.33**

Table 4: IoU for every class of Paris-Lille-3D dataset

Method	Tree	Low vege.	Car	Facade	Road	Sidewalk	Pole	Other
SPG	81.27	38.87	**97.17**	96.44	79.36	2.91	**67.69**	**58.56**
DGCNN	91.63	65.28	87.10	95.83	95.70	79.33	63.16	50.95
PointNLM	**94.39**	**75.30**	89.20	**96.60**	**96.50**	**82.56**	51.31	56.80

In addition, we output 8 category prediction scores for each super voxel before the softmax layer. Based on these prediction scores, we calculate the True Positive Rate (TPR), and False Positive Rate (FPR) under different threshold by the following two formulas:

$$\mathrm{TPR} = \frac{TP}{TP + FN} \tag{7}$$

$$\mathrm{FPR} = \frac{FP}{FP + TN} \tag{8}$$

where TP is the number of true positive supervoxel, FP is the number of false positive supervoxel, FN and TN are the false negative and true negative supervoxel. Then, the macro-averaging ROC curve is plotted by the Scikit-learn.

Compared with the state-of-the-art point cloud network, DGCNN, our method achieves more high true positive and low false positive rates in the Paris-Lille-3D dataset with multiple authentication as shown in Fig.13.

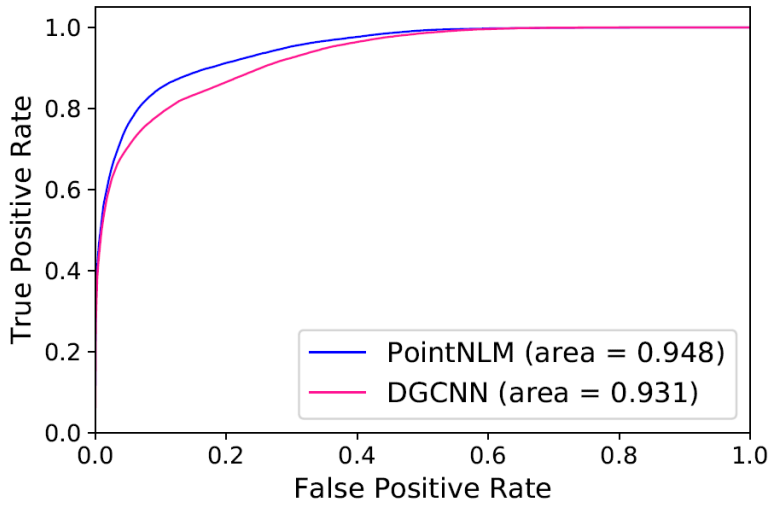

Fig. 13. ROC curve of two different network on Paris-Lille-3D datasets.

4.4. large-scale data segmentation results

We used the test dataset with several large-scale point cloud scenes. Each scene spans approximately 200m and includes tens of millions of points along the road. These data, which have point clouds with RGB color information, were obtained from Germany. For this data, instead of retraining the network model, we directly used the PointNLM network model trained by the Semantic 3D dataset to segment the tree domain. Fig. 14 shows the results of tree segmentation in three large-scale spot cloud scenes. As seen from the figure, for trees of different shapes, sizes, and connected areas, our algorithm has great advantages over previous works. Current computing capability makes it possible to scale the scenarios to the maximum extent. For this large-scale data, the Table 5 shows IoU of the tree and other objects as well as mean IoU.

Table 5: The IoU of large-scale data

Tree	Other objects	mean IoU
0.875	0.958	0.916

(a)

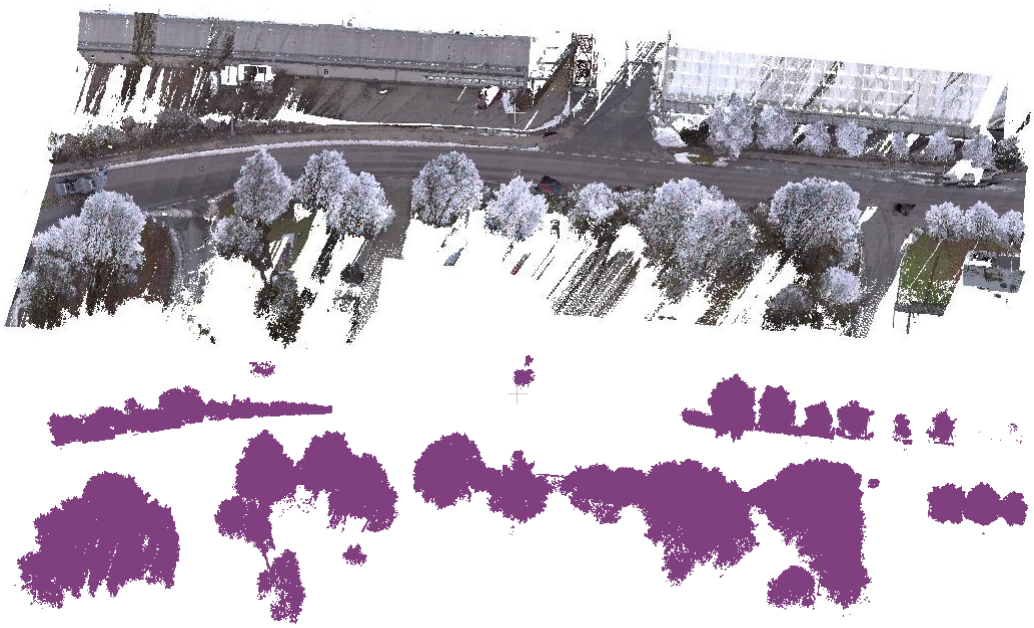

(b)

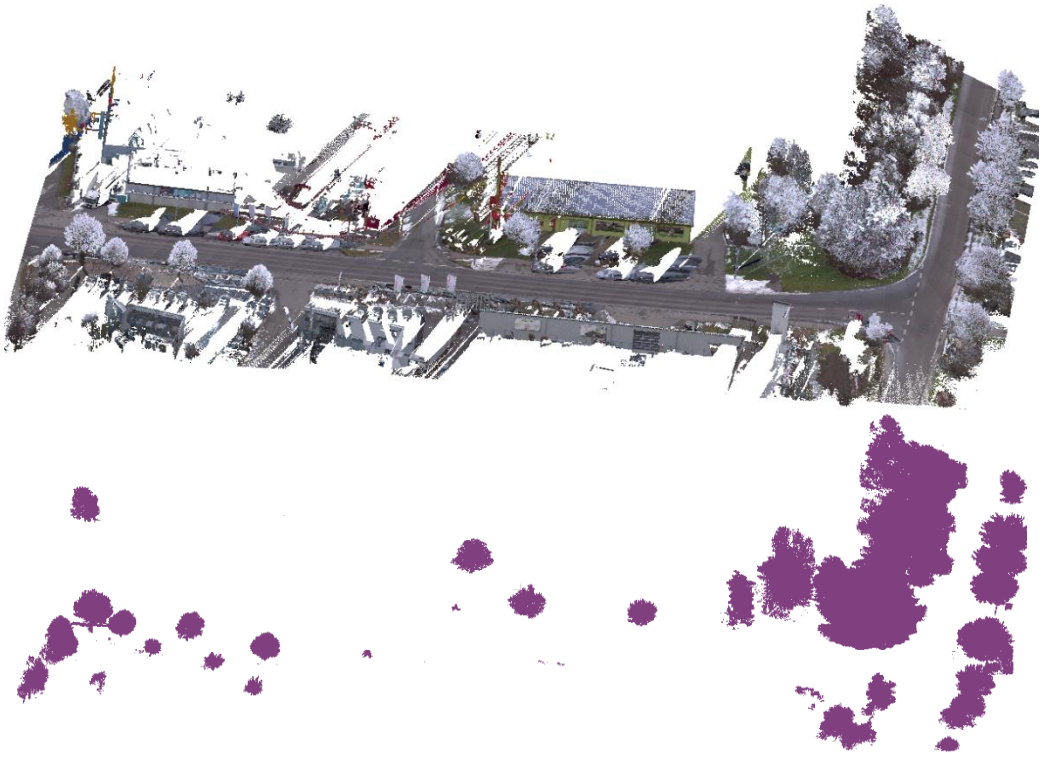

(c)

Fig. 14. Quantitative results: tree segmentation results of three scenes

5. Conclusion

We presented a new approach to detect and extract vegetation in urban areas using TLS data. Two important contributions are summarized as follows: (1) adoption via the middle echo to detect part of the vegetation prior to identification. (2) create a Nonlocal Means network to capture the relationship between long-range supervoxels and finish the fine segmentation of trees. Within the network, a network module that implements max-pooling in a disordered point cloud was designed, resulting in the network having a wider receptive field and capturing high-level features of point cloud distribution.

The presented approach was evaluated using the Semantic 3D small test dataset. The IoU of tree segmentation, 0.864, is already higher than that of many semantic segmentation networks, indicating that our tree segmentation algorithm is effective. In addition, we also evaluated the segmentation performance of our Nonlocal means network using the Paris-Lille-3D dataset. The average IoU of 0.803, for our segmentation on the twelve sections of the Paris-Lille-3D dataset,

is not only much higher than the 0.65 achieved by the SPGraph network, but is also higher than the 0.79 for DGCNN.

Acknowledgements

This work was supported by the National Natural Science Foundation of China under Grants No.61601392 and No.41871380. In this study, thanks Dr. Michael Mcallister for helpful advising in writing.

References

Babahajiani, P., Fan, L., Kämäräinen, J.-K., Gabbouj, M., 2017. Urban 3D segmentation and modelling from street view images and LiDAR point clouds. Machine Vision and Applications 28, 679–694.

Boulch, A., Le Saux, B., Audebert, N., 2017. Unstructured Point Cloud Semantic Labeling Using Deep Segmentation Networks., in: 3DOR.

Demantké, J., Mallet, C., David, N., Vallet, B., 2011. Dimensionality based scale selection in 3D lidar point clouds. International Archives of Photogrammetry, Remote Sensing and Spatial Information Sciences, Laser Scanning 2011.

Gross, H., Jutzi, B., Thoennessen, U., 2007. Segmentation of tree regions using data of a full-waveform laser. International Archives of Photogrammetry, Remote Sensing and Spatial Information Sciences 36, W49A.

Guan, H., Yu, Y., Ji, Z., Li, J., Zhang, Q., 2015. Deep Learning-Based Tree Classification Using Mobile LiDAR Data. Remote Sensing Letters 6, 864–873. https://doi.org/10.1080/2150704X.2015.1088668

Hackel, T., Savinov, N., Ladicky, L., Wegner, J.D., Schindler, K., Pollefeys, M., 2017. SEMANTIC3D.NET: A new large-scale point cloud classification benchmark, in: ISPRS Annals of the Photogrammetry, Remote Sensing and Spatial Information Sciences. pp. 91–98.

Hollaus, M., Mücke, W., Höfle, B., Dorigo, W., Pfeifer, N., Wagner, W., Bauerhansl, C., Regner, B., 2009. Tree species classification based on full-waveform airborne laser scanning data. Proceedings of SILVILASER 14–16.

Hua, B.-S., Tran, M.-K., Yeung, S.-K., 2018. Pointwise convolutional neural networks, in: Proceedings of the IEEE Conference on Computer Vision and Pattern Recognition. pp. 984–993.

Huang, P., Chen, Y., Li, J., Yu, Y., Wang, C., Nie, H., 2015. Extraction of street trees from mobile laser scanning point clouds based on subdivided dimensional features, in: Geoscience and Remote Sensing Symposium. pp. 557–560.

Klokov, R., Lempitsky, V., 2017. Escape from Cells: Deep Kd-Networks for the Recognition of 3D Point Cloud Models. IEEE, pp. 863–872. https://doi.org/10.1109/ICCV.2017.99

Landrieu, L., Simonovsky, M., 2018. Large-scale point cloud semantic segmentation with superpoint graphs, in: Proceedings of the IEEE Conference on Computer Vision and Pattern Recognition. pp. 4558–4567.

Liu, J., Xiao, Z., Chen, Y., Huang, P., Wu, R., Li, J., 2017. Automated extraction of urban roadside trees from mobile laser scanning point clouds based on a voxel growing method, in: IGARSS 2017 - 2017 IEEE International Geoscience and Remote Sensing Symposium. pp. 1832–1835.

Luo, H., Wang, C., Wen, C., Chen, Z., Zai, D., Yu, Y., Li, J., 2018. Semantic Labeling of Mobile LiDAR Point Clouds via Active Learning and Higher Order MRF. IEEE Transactions on Geoscience and Remote Sensing 56, 3631–3644. https://doi.org/10.1109/TGRS.2018.2802935

Luo, Z., Li, J., Xiao, Z., Mou, Z.G., Cai, X., Wang, C., 2019. Learning High-Level Features by Fusing Multi-View Representation of MLS Point Clouds for 3D Object Recognition in Road Environments. ISPRS Journal of Photogrammetry and Remote Sensing 150, 44–58. https://doi.org/10.1016/j.isprsjprs.2019.01.024

Maturana, D., Scherer, S., 2015. Voxnet: A 3D convolutional neural network for real-time object recognition, in: Intelligent Robots and Systems (IROS), 2015 IEEE/RSJ International Conference On. IEEE, pp. 922–928.

Qi, C. R., Su, H., Mo, K., Guibas, L.J., 2017a. Pointnet: Deep learning on point sets for 3D classification and segmentation. Proc. Computer Vision and Pattern Recognition (CVPR), IEEE 1, 4.

Qi, C. R., Yi, L., Su, H., Guibas, L.J., 2017b. Pointnet++: Deep hierarchical feature learning on point sets in a metric space, in: Advances in Neural Information Processing Systems. pp. 5099–5108.

Riegler, G., Osman Ulusoy, A., Geiger, A., 2017. Octnet: Learning deep 3D representations at high resolutions, in: Proceedings of the IEEE Conference on Computer Vision and Pattern Recognition. pp. 3577–3586.

Roynard, X., Deschaud, J.E., Goulette, F., 2017. Paris-Lille-3D: a large and high-quality ground truth urban point cloud dataset for automatic segmentation and classification. International Journal of Robotics Research 027836491876750.

Su, H., Maji, S., Kalogerakis, E., Learned-Miller, E., 2015. Multi-view convolutional neural networks for 3D shape recognition, in: Proceedings of the IEEE International Conference on Computer Vision. pp. 945–953.

Te, G., Hu, W., Guo, Z., Zheng, A., 2018. RGCNN: Regularized Graph CNN for Point Cloud Segmentation. arXiv preprint arXiv:1806.02952.

Vosselman, G., Maas, H.-G. (Eds.), 2011. Airborne and Terrestrial Laser Scanning, repr. ed. Whittles, Dunbeath.

Wang, C., Samari, B., Siddiqi, K., 2018. Local spectral graph convolution for point set feature learning, in: Proceedings of the European Conference on Computer Vision (ECCV). pp. 52–66.

Wang, Y., Sun, Y., Liu, Z., Sarma, S.E., Bronstein, M.M., Solomon, J.M., 2018. Dynamic graph CNN for learning on point clouds. arXiv preprint arXiv:1801.07829.

Weinmann, M., Jutzi, B., Hinz, S., Mallet, C., 2015. Semantic point cloud interpretation based on optimal neighborhoods, relevant features and efficient classifiers. ISPRS Journal of Photogrammetry and Remote Sensing 105, 286–304.

Weinmann, Martin, Weinmann, Michael, Mallet, C., Brédif, M., 2017. A Classification-Segmentation Framework for the Detection of Individual Trees in Dense MMS Point Cloud Data Acquired in Urban Areas. Remote Sensing 9, 277. https://doi.org/10.3390/rs9030277

Wu, B., Yu, B., Wu, Q., Huang, Y., Chen, Z., Wu, J., 2016. Individual tree crown delineation using localized contour tree method and airborne LiDAR data in coniferous forests. International Journal of Applied Earth Observation and Geoinformation 52, 82–94.

Xu, Sheng, Xu, Shanshan, Ye, N., Zhu, F., 2018a. Individual stem detection in residential environments with MLS data. Remote Sensing Letters 9, 51–60. https://doi.org/10.1080/2150704X.2017.1384588

Xu, Sheng, Xu, Shanshan, Ye, N., Zhu, F., 2018b. Automatic extraction of street trees' nonphotosynthetic components from MLS data. International Journal of Applied Earth Observation and Geoinformation 69, 64–77.

Yang, B., Dong, Z., 2013. A shape-based segmentation method for mobile laser scanning point clouds. ISPRS Journal of Photogrammetry and Remote Sensing 81, 19–30.

Yang, B., Dong, Z., Zhao, G., Dai, W., 2015. Hierarchical extraction of urban objects from mobile laser scanning data. ISPRS Journal of Photogrammetry and Remote Sensing 99, 45–57.

Yu, Y., Li, J., Yu, J., Guan, H., Wang, C., 2013. Pairwise Three-Dimensional Shape Context for Partial Object Matching and Retrieval on Mobile Laser Scanning Data. IEEE Geoscience and Remote Sensing Letters 11, 1019–1023.

Zou, X., Cheng, M., Wang, C., Xia, Y., Li, J., 2017. Tree classification in complex forest point clouds based on deep learning. IEEE Geoscience and Remote Sensing Letters 14, 2360–2364.